Modified Scaled Hierarchical Equation of Motion Approach for the Study of Quantum Coherence in Photosynthetic Complexes

Jing Zhu and Sabre Kais*

Department of Chemistry and Birck Nanotechnology Center, Purdue University, West Lafayette, Indiana 47907, United States

Patrick Rebentrost and Alán Aspuru-Guzik

Department of Chemistry and Chemical Biology, Harvard University, 12 Oxford Street, Cambridge, Massachusetts 02138, United States

ABSTRACT: We present a detailed theoretical study of the transfer of electronic excitation energy through the Fenna–Matthews–Olson (FMO) pigment–protein complex, using the newly developed modified scaled hierarchical approach (Shi, Q.; et al. *J. Chem. Phys.* **2009**, *130*, 084105). We show that this approach is computationally more efficient than the original hierarchical approach. The modified approach reduces the truncation levels of the auxiliary density operators and the correlation function. We provide a systematic study of how the number of auxiliary density operators and the higher-order correlation functions affect the exciton dynamics. The time scales of the coherent beating are consistent with experimental observations. Furthermore, our theoretical results exhibit population beating at physiological temperature. Additionally, the method does not require a low-temperature correction to obtain the correct thermal equilibrium at long times.
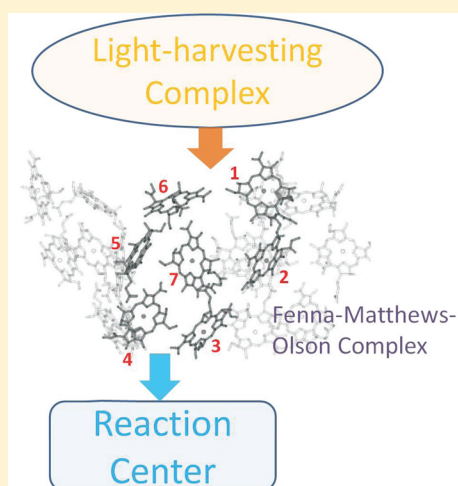
I. INTRODUCTION

In the initial step of photosynthesis, light is captured by protein-bound pigments that are part of light-harvesting antenna complexes. The excitation energy is transferred with a near-unity quantum yield to reaction centers, where it is converted to chemical energy. The underlying molecular mechanisms responsible for the near-unity quantum yield are far from being understood. In this regard, an extensively studied and relevant system is the Fenna–Matthews–Olson (FMO) pigment–protein complex of green-sulfur bacteria, which acts as a mediator of excitation energy between the outer antenna system, i.e., the chlorosomes, and the reaction center.[1]

Experimentally, Savikhin et al.[2] observed quantum beating in the FMO complex using the fluorescence anisotropy technique. More recently, Engel et al.[3] employed two-dimensional electronic spectroscopy to observe long-lasting quantum beats that provides direct evidence for survival of long-lived electronic coherence for hundreds of femtoseconds. Aspuru-Guzik et al.[4−6] investigated the effects of quantum coherence and the fluctuating environment, using the Lindblad formalism, on the enhancement of the photosynthetic electronic energy transfer efficiency from the perspective of a quantum walk. In Rebentrost et al.,[6] a method to quantify the role of quantum coherence was introduced.

Ishizaki et al.[7−9] employed the hierarchical equation of motion (HEOM) approach expansion in order to address the robustness and the role of the quantum coherence under physiological conditions. Their results reveal that quantum wave-like motion persists for several hundred femtoseconds even at physiological temperature $T = 300$ K. Very recently, a very large-scale calculation of energy transfer between chromophore rings of purple bacteria was carried out using the HEOM approach.[10] Meanwhile, Whaley et al.[11] and Caruso et al.[12] discussed quantum entanglement in photosynthetic harvesting complexes and clarified the connection between coherence and entanglement. They showed that the FMO complex exhibits bipartite entanglement between dimerized chromophores. The subject continues to be of great interest with a large number of publications discussing electronic energy transfer in photosynthetic complexes, in particular, the issue of quantum speed-up in the FMO complex.[13−19]

In this paper, we present a detailed theoretical study of the transfer of excitation energy toward the reaction center through the Fenna–Matthews–Olson (FMO) pigment–protein complex

using a modified scaled hierarchy equation of motion approach, which was developed by Shi and co-workers recently.[20] This approach guarantees that the auxiliary density operators decay to zero at high truncation level. Furthermore, it provides a considerable computational speed-up over the original hierarchical approach.[7] We will show that the scaled hierarchical approach can reduce the truncation level of both auxiliary density operators and the correlation functions compared to the classical approach. The time scales of the coherent beating are consistent with experimental observations. Furthermore, our results show that the population beating persists at physiological temperature.

II. THEORY

Excitonic energy transfer within photosynthetic proteins, such as the FMO complex, operates in a demanding parameter regime where a small perturbative quantity is not available. It is thus a challenge to find accurate and efficient methods for the simulation of the quantum dynamics. A number of approximate methods have been developed:[16] they include the semiclassical Förster theory, standard Redfield theory, modified Redfield theories, the modified Lindblad formalism, and hierarchical equations of motion, among others.[4,21,22]

In this study, we utilize the recent hierarchical Liouville space propagator method developed by Shi et al.[20] to investigate excitation energy transfer in the FMO complex. The original method is based on a reformulation of the original hierarchical quantum master equation and the incorporation of a filtering algorithm that automatically truncates the hierarchy with a preselected tolerance. They showed how this method significantly reduces the number of auxiliary density operators used to calculate electron transfer dynamics in a spin-boson model and the absorption spectra of an excitonic dimer.[20]

The structure of the FMO complex was first analyzed by Fenna and Matthews in 1975.[23] It consists of a trimer, formed by three identical monomers. Each monomer contains seven bacteriochlorophyll a (BChl a) molecules (or seven "sites"). Biologically, the FMO complex acts as a molecular energy wire, transferring excitation energy from the chlorosome structure, where light is captured, to the reaction center (RC). There is substantial evidence that the FMO complex is oriented such that sites 1 and 6 are close to the baseplate protein and sites 3 and 4 are close to the RC complex and thus define the target region for the exciton.[16,23−25] The detailed structure is shown in Figure 1. It should be mentioned that the presence of the eighth BChl a molecule per monomer was proposed by Ben-Shem et al. in 2004.[26] This has been verified experimentally recently by Tronrud and co-workers.[27] It has been suggested that the eighth BChl a molecule acts as a gateway site from the reaction center to the 27 chromophores in the trimer.[27]

The total Hamiltonian of the quantum system is given by

$$\mathscr{H} = \mathscr{H}_S + \mathscr{H}_B + \mathscr{H}_{SB} \tag{1}$$

where $\mathscr{H}_S$, $\mathscr{H}_B$, and $\mathscr{H}_{SB}$ are the Hamiltonians of the system, the environment, and the system−environment coupling, respectively. Here, we consider each site as a two-level system of ground state and excited state. The system Hamiltonian, $\mathscr{H}_S$, which describes the electronic states of the pigments can be expressed as

$$\mathscr{H}_S = \sum_{j=1}^{N} \varepsilon_j |j\rangle\langle j| + \sum_{j<k} J_{jk}(|j\rangle\langle k| + |k\rangle\langle j|) \tag{2}$$
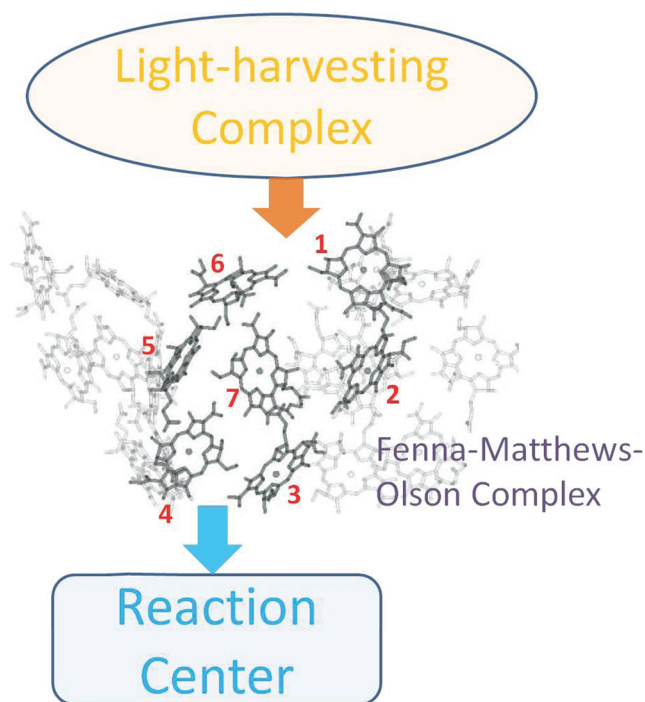

Figure 1. Sketch of the energy flow in the process of photosynthesis. The energy is captured by the light-harvesting complex (LHC) and transferred to the reaction center (RC). The FMO complex is the link between LHC and RC, and it operates as a "wire" during the energy transfer process. Using the convention for numbering the BChl a molecules (sites) of the FMO complex as in ref 23, sites 1 and 6 are close to the LHC and sites 3 and 4 are close to the RC. In our theoretical description, the excited states of the BChl a molecules of the FMO complex are considered as the "system" and all the other relevant degrees of freedom are referred to as the "environment".

$|j\rangle$ denotes the state where only the jth site is in its excited state and all other sites are in their ground state. ε_j represents the site energy of the jth site which is defined as the optical transition energy at the equilibrium configuration of environmental phonons associated with the ground state. N is the number of pigments or sites. J_{jk} is the electronic coupling between sites j and k. The parameters for this Hamiltonian are taken from the paper of Adolphs and Renger.[28] In their work, two independent methods were used to obtain the site energies of the seven BChl a molecules of the monomeric subunits of the FMO complex. In the first method, the site energies are used as parameters that were optimized by a genetic algorithm in the fit of the optical spectra. In the second one, the site energies are obtained directly by electrochromic shift calculations.[28]

For the Hamiltonian of the environment, $\mathscr{H}_B$, a harmonic oscillator model is applied. Furthermore, it is assumed that the electronic excitation on each site couples to its own bath independently:

$$\mathscr{H}_B = \sum_{j=1}^{N} \mathscr{H}_B^j = \sum_{j=1}^{N} \sum_{\xi=1}^{N_{jB}} \frac{P_{j\xi}^2}{2m_{j\xi}} + \frac{1}{2} m_{j\xi} \omega_{j\xi}^2 x_{j\xi}^2 \tag{3}$$

where N_{jB} is the number of different harmonic modes coupled to the jth site. Here, $m_{j\xi}$, $\omega_{j\xi}$, $P_{j\xi}$, and $x_{j\xi}$ are the mass, frequency, momentum, and position operator of the harmonic bath modes. The coupling term, $\mathscr{H}_{SB}$, which is responsible for fluctuations in

the site energies by the phonon dynamics, can be expressed as

$$\mathcal{H}_{\mathrm{SB}} = \sum_{j=1}^{N} \mathcal{H}_{\mathrm{SB}}^{j} = -\sum_{j=1}^{N} |j\rangle\langle j| \cdot F_j = -\sum_{j=1}^{N} \mathcal{V}_j \cdot F_j \quad (4)$$

where the bath part is $F_j = \sum_{\xi} c_{j\xi} \cdot x_{j\xi}$ and $c_{j\xi}$ represents the system–environment coupling constant for the jth site and ξth phonon mode. The projection operator $\mathcal{V}_j = |j\rangle\langle j|$ describes the system part of the interaction.

At time $t = 0$, we assume that the system and the environment are decoupled, i.e., $\rho_{\mathrm{tot}}(0) = \rho(0) \otimes \rho_{\mathrm{B}}(0)$. Additionally, the environment is in the Boltzmann equilibrium state, $\rho_{\mathrm{B}}(0) = e^{-\beta H_{\mathrm{B}}}/\mathrm{Tr}_{\mathrm{B}}[e^{-\beta H_{\mathrm{B}}}]$, where $\beta = 1/k_{\mathrm{B}}T$. The time evolution of the system density matrix, $\rho(t)$, can be calculated by tracing out the environment degrees of freedom:

$$\rho(t) = \mathrm{Tr}_{\mathrm{B}}[\rho_{\mathrm{tot}}(t)] = \mathrm{Tr}_{\mathrm{B}}[e^{-i\mathcal{H}t/\hbar}\rho_{\mathrm{tot}}(0)e^{i\mathcal{H}t/\hbar}] \quad (5)$$

The bath is described by its correlation functions, $C_j(t)$, which are defined as[10,29,30] $C_j(t) = \mathrm{Tr}_{\mathrm{B}}[\tilde{F}_j(t)\tilde{F}_j(0)\rho_{\mathrm{B}}]$, where the Langevin force, $\tilde{F}_j(t)$, is given in the interaction picture: $\tilde{F}_j(t) = e^{i\mathcal{H}_{\mathrm{B}}t/\hbar}F_j e^{-i\mathcal{H}_{\mathrm{B}}t/\hbar}$. For the phonon bath, the correlation function can be written as $C_j(t) = (1/\pi)\int_{-\infty}^{\infty}d\omega \cdot J_j(\omega) \cdot [e^{-i\omega t}/1 - e^{-\beta\hbar\omega}]$, where $J_j(\omega)$ is the spectral density for the jth site:

$$J_j(\omega) = \sum_{\xi} \frac{c_{j\xi}^2 \cdot \hbar}{2m_{j\xi} \cdot \omega_{j\xi}} \delta(\omega - \omega_{j\xi}) \quad (6)$$

To proceed, we use the Drude spectral density, which corresponds to an overdamped Brownian oscillator model. Furthermore, we assume that the system–environment coupling is the same for all sites, $J_j(\omega) = J(\omega)$, $\forall$ js. The Drude spectral density is defined as

$$J(\omega) = \eta\gamma\frac{\omega}{\omega^2 + \gamma^2} \quad (7)$$

We introduced $\eta = 2\lambda/\hbar$, which is dependent on the reorganization energy, λ, and the Drude decay constant, γ. Under this spectral density, the correlation function $C_j(t)$ takes the form

$$C_j(t > 0) = \sum_{k=0}^{\infty} c_k \cdot e^{-v_k t} \quad (8)$$

with the Matsuraba frequencies $v_0 = \gamma$ and $v_k = 2k\pi/\beta\hbar$ for $k \geqslant 1$. The constants c_k are given by

$$c_0 = \frac{\eta\gamma}{2}\left[\cot\left(\frac{\beta\hbar\gamma}{2}\right) - i\right]$$

$$c_k = \frac{2\eta\gamma}{\beta\hbar} \cdot \frac{v_k}{v_k^2 - \gamma^2} \quad \text{for} \quad k \geqslant 1$$

Now, we are in the position to write down the HEOM for the reduced density operator[10]

$$\frac{\mathrm{d}}{\mathrm{d}t}\rho_n = -(i\mathcal{L}_{\mathrm{S}} + \sum_{j=1}^{N}\sum_{k} n_{jk}v_k)\rho_n - i\sum_{j=1}^{N}[\mathcal{V}_j, \sum_{k}\rho_{n_{jk}^+}]$$

$$-i\sum_{j=1}^{N}\sum_{k} n_{jk}(c_k\mathcal{V}_j\rho_{n_{jk}^-} - c_k^*\rho_{n_{jk}^-}\mathcal{V}_j) \quad (9)$$

where n denotes the set of nonnegative integers $n \equiv \{n_1, n_2, \ldots, n_N\} = \{\{n_{10}, n_{11}, \ldots, n_{1K}\}, \ldots, \{n_{N0}, n_{N1}, \ldots, n_{NK}\}\}$. $n_{jk}^{\pm}$ refers to the

change of the number n_{jk} to $n_{jk} \pm 1$ in the global index n. The sum of n_{jk} is called tier $\mathcal{N}_{\mathrm{c}}$, $\mathcal{N}_{\mathrm{c}} = \sum_{j,k} n_{jk}$. In particular, $\rho_0 = \rho_{\{\{0,0,\ldots\},\ldots,\{0,0,\ldots\}\}}$ is the system's reduced density operator (RDO) and all others are auxiliary density operators (ADOs). Although the RDO is the most important operator, the ADOs contain corrections to the system–environment interaction; these arised from the nonequilibrium treatment of the bath.

Here, we assume that both ρ_0 and $\mathcal{V}_j$ have the order of 1. When the tier of ρ_n at tier $\mathcal{N}_{\mathrm{c}}$ ($\mathcal{N}_{\mathrm{c}} = \sum_{j,k} n_{jk}$), the amplitude of ρ_n is proportional to $|c_0^{\sum_j n_{j0}} c_1^{\sum_j n_{j1}} \ldots c_K^{\sum_j n_{jK}}|$ following the standard approach (eq 9),[31,32] which indicates the amplitude of ρ_n is related to both c_k and n_{jk}. n_{jk} is decided by the truncation level, while c_k is related to the correlation function. The correlation function is derived from the system–environment correlation. In other words, the amplitude of ρ_n is dependent on the system–environment coupling. Under the intermediate-to-strong system–environment coupling, the amplitude of ρ_n cannot be guaranteed to be small even at high truncation level. It goes to the opposite direction as we expected, since we always expect more accurate results at high truncation level. Fortunately, Shi and co-workers developed a new approach in which one is able to rescale the original ADOs which can be used for overcoming this issue.[20] They scaled the original operator as

$$\tilde{\rho}_n(t) = \left(\prod_{k,j} n_{jk}!|c_k|^{n_{jk}}\right)^{-1/2}\rho_n(t) \quad (10)$$

After the scaling, $|\tilde{\rho}_n|$ has the order of $\prod_{k,j}(|c_k|^{n_{jk}}/n_{jk}!)^{1/2}$. It can make sure that $|\tilde{\rho}_n|$ decays to zero at higher hierarchical truncation level.

Since the number of contributing terms to the correlation function, eq 8, and ADOs is infinite, the computation of eq 9 is—in general—impossible. In order to overcome this problem, a truncation scheme for both the correlation function and ADOs is applied. We set the truncation level for the correlation function (Matsuraba frequency and constant c_k) at level K, while the cutoff for the tier of ADOs is $\mathcal{N}_{\mathrm{c}}$. With the Ishizaki–Tanimura truncating scheme,[31,32] eq 9 for the scaled density operator becomes

$$\frac{\mathrm{d}}{\mathrm{d}t}\tilde{\rho}_n = -(i\mathcal{L}_{\mathrm{S}} + \sum_{j=1}^{N}\sum_{k=0}^{K} n_{jk}v_k)\tilde{\rho}_n$$

$$-i\sum_{j=1}^{N}\sum_{k}\sqrt{(n_{jk}+1)|c_k|}[\mathcal{V}_j, \tilde{\rho}_{n_{jk}^+}]$$

$$-\sum_{j=1}^{N}\sum_{m=K+1}^{\infty}\frac{c_{jm}}{v_{jm}} \times [\mathcal{V}_j, [\mathcal{V}_j, \tilde{\rho}_n]]$$

$$-i\sum_{j=1}^{N}\sum_{k=0}^{K}\sqrt{n_{jk}/|c_k|}(c_k\mathcal{V}_j\tilde{\rho}_{n_{jk}^-} - c_k^*\tilde{\rho}_{n_{jk}^-}\mathcal{V}_j) \quad (11)$$

We use eq 11 to simulate the exciton dynamics of the FMO complex.

III. RESULTS AND DISCUSSION

For the numerical analysis, we used the same Hamiltonian as in refs 7 and 28, the same reorganization energy, $\lambda_j = \lambda = 35$ cm^{-1}, and the Drude decay constant, $\gamma_j^{-1} = \gamma^{-1} = 50$ fs, of
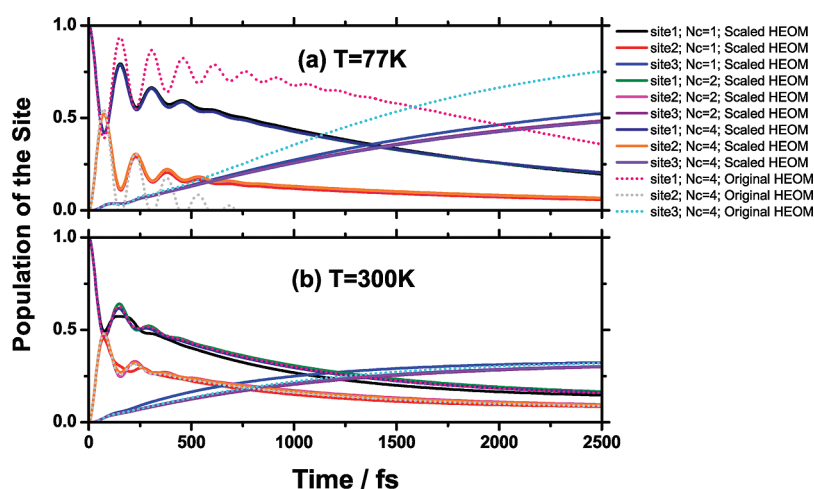
Figure 2. The population evolution of sites 1, 2, and 3 under different cutoffs for the tier of auxiliary density operator ($\mathcal{N}_c$) and different HEOM approaches. The solid lines represent the population evolution at three different truncation levels $\mathcal{N}_c = 1$, 2, and 4 of the scaled HEOM approach. The short dotted lines show the time evolution of $\mathcal{N}_c = 4$ at the original HEOM approach. Site 1 is initially excited, and the reorganization energy and Drude decay constant are $\lambda_j = \lambda = 35$ cm^{-1} and $\gamma_j^{-1} = \gamma^{-1} = 50$ fs, respectively. The dynamics are shown at cryogenic temperature $T = 77$ K (upper panel) and at physiological temperature $T = 300$ K (lower panel).

refs 7 and 33. As we mentioned before, sites 1 and 6 are both connected to the LHC. It is possible that site 1, site 6, or both sites are excited. For this reason, three different initial conditions are employed, $|1\rangle$ (site 1 is excited), $|6\rangle$ (site 6 is excited), and $1/(2)^{1/2}(|1\rangle + |6\rangle)$ (the superposition of excited sites 1 and 6).

Calibration. We compare the scaled approach to the original HEOM approach and investigate the critical choice of the truncation levels of ADOs ($\mathcal{N}_c$) and the correlation functions (K). The original HEOM approach is given in eq 9. In Figure 2, we depict the population of sites 1, 2, and 3 for different N_c in the scaled approach and for $N_c = 4$ in the original approach at temperatures $T = 77$ K and $T = 300$ K, setting $K = 0$. One obtains a large difference between the two approaches at $T = 77$ K; see the dotted lines in the figure. Under the original HEOM method, the population of site 2 goes below 0 after 750 fs, which is unphysical. However, the population of each site under the scaled HEOM approach behaves reasonably even at $\mathcal{N}_c = 1$. This shows that the scaled HEOM approach can result in better simulation results at less computational costs. The difference between the two approaches originates from the truncation level of the correlation function, which is due to the coupling between the system and the environment.

For the scaled approach itself, the difference between different truncation levels ($\mathcal{N}_c$) is modest at both temperatures. It can be seen that there is only minimal difference among three $\mathcal{N}_c$ values at $T = 77$ K. Beyond 1500 fs, the difference of the population evolution for site 3 becomes larger between the case of $\mathcal{N}_c = 1$ and $\mathcal{N}_c = 2$ and 4. The population evolution of all the sites is exactly the same for $\mathcal{N}_c = 2$ and 4. As a result, $\mathcal{N}_c \geq 2$ is the sufficient truncation level for the ADOs at $T = 77$ K. At room temperature, $T = 300$ K, the variation at the dynamics of the populations as a function of $\mathcal{N}_c$ is more apparent. The population evolution of all sites for $\mathcal{N}_c = 1$ is not as smooth as in the other two situations. For the cases of $\mathcal{N}_c = 2$ and 4, there is a slight difference in the population beatings which occur between 200 and 300 fs. Although this is not a substantial difference, we believe $\mathcal{N}_c = 4$ is a good compromise between efficiency and accuracy.

For the truncation level of the correlation function (K), the simulation for the seven sites is computationally unwieldy.

Therefore, we truncated the system to test the correlation truncation level using a three-site model (sites 1, 2, and 3) with three different values of K, being $K = 0$, 1, and 2. The results show that truncation level $K = 0$ is enough for both $T = 77$ and 300 K. A similar result was also found in ref 20, where nonzero K was shown to be significant in the dynamics only at rather long time scales. In the following computations, we chose $\mathcal{N}_c = 4$ for both temperatures as our reference. At this point, we would like to emphasize the numerical efficiency of the scaled HEOM approach. The original HEOM approach requires a truncation level as high as $\mathcal{N}_c = 12$ to get converged results.[7] However, we only require $\mathcal{N}_c = 2$ for $T = 77$ K and $\mathcal{N}_c = 4$ for $T = 300$ K, which is a significant resource reduction. On a standard desktop computer, a simulation of the time evolution for 2.5 ps takes about 7 min for the case of $\mathcal{N}_c = 2$ and about 1.5 h for the case of $\mathcal{N}_c = 4$.

Coherent Beatings at Cryogenic and Room Temperatures. Now, we investigate the cryogenic temperature $T = 77$ K in more detail. This is the temperature of the first experiment by Engel et al.[3] which shows coherent phase evolution of the FMO complex from time $t = 0$ to roughly $t = 660$ fs. The results are presented in Figure 3. In the left panel, we show the results of simulation for the system Hamiltonian only. In the right panel, one can observe that the quantum beating between certain sites clearly persists in the short time dynamics of the full FMO complex. For the simulated initial conditions, the population beatings can last for hundreds of femtoseconds; this time scale is in agreement with the experimental observation.[3] The population beating for all three different initial conditions can last around 650 fs. In Figure 3a, the initial state is localized at site 1. The system exhibits coherent beatings between the strongly coupled sites 1 and 2, accompanied by relatively slow relaxation to sites 3 and 4. The change of population of all other sites is weak. In Figure 3b, where the initial state is localized at site 6, the population relaxes faster. For $t \leq 400$ fs, there is population beating between the strongly coupled sites 6 and 5, accompanied by relaxation to the intermediate sites 4, 5, and 7. From these sites, the population is fed into the low-energy sites 3 and 4. The population of site 6 almost vanishes at $t = 800$ fs, while for the previous initial condition, Figure 3a, the population of site 1 is roughly 0.5 at that time.
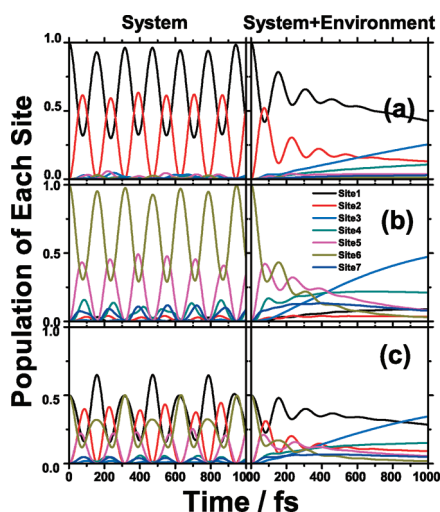
Figure 3. Population evolution of each site at cryogenic temperature T = 77 K. The left panel shows the dynamics for the system alone, and the right includes the effects of the environment. The reorganization energy is $\lambda_j = \lambda = 35$ cm^{-1}, while the value of the Drude decay constant is $\gamma_j^{-1} = \gamma^{-1} = 50$ fs. The initial conditions are site 1 excited (a), site 6 excited (b), and the superposition of sites 1 and 6 (c).

The exciton migration pathways and time scales are in accordance with previous work.[7,13,28] Finally, Figure 3c represents the superposition of sites 1 and 6. The time evolution of this case is the combination of the single site excited cases. That is, the population evolution on site 1 follows the pathway of initially single site 1 excited, while the pathways for the population on site 6 are the same as the single site 6 excited case.

In order to investigate the excitation transfer beyond the initial beating region, we extended the simulation to a longer time (~2500 fs). The results are shown in Figure 5. To check whether the entire system converges to the thermal equilibrium, we obtained all eigenvalues of the system Hamiltonian and calculated the probability of each eigenstate under temperature T based on the Boltzmann distribution. Subsequently, we transformed the population from the eigenstate representation to site representation and obtained the population of each site at thermal equilibrium. At T = 77 K, the population of site 3 is 0.69 and that of site 4 is 0.22. The population of all other sites is smaller than 0.03. For the case of having the initial excitation start in site 6, the thermal equilibrium reached the end of 2 ps, while for the case of the other two initial conditions, they are still on their way to the thermal equilibrium at the end of 2.5 ps. Our simulation shows that the system reaches thermal equilibrium at ~7 ps for the case in which site 1 was initially excited and the time for the initial superposition of sites 1 and 6 is around 6 ps.

A recent experiment studied the excitation dynamics of the FMO complex at room temperature.[34] To investigate quantum coherence effects under physiological conditions, we simulate the dynamics at the temperature T = 300 K. We chose three different values for γ^{-1} in our calculation: 50, 100, and 166 fs.[7,9] Following the same procedure as before, we consider three different initial conditions with the reorganization energy λ = 35 cm^{-1}. We choose the truncation level at $\mathcal{N}_c$ = 4. The calculation results are shown in Figure 6.

The main difference between the case of 300 K and that of 77 K is the time scale of the persistence of population beating. The coherent beating lasts only 400 fs at room temperature, whereas it lasts much longer at T = 77 K. It is also found that the
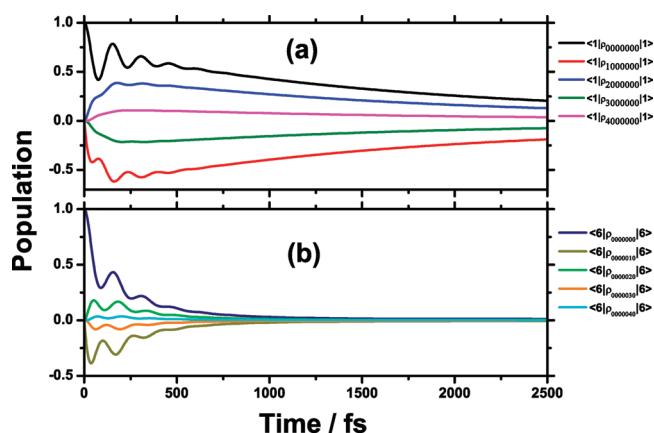

Figure 4. Population evolution of the RDO and ADOs for the case of initial excitation at sites 1 and 6, respectively. The first panel shows the time evolution of the ADO $\langle 1|\rho_{n000000}|1\rangle$ elements with n = 0, 1, 2, 3, and 4. The second panel shows the time evolution of the $\langle 6|\rho_{00000m0}|6\rangle$ elements with levels of truncation m = 0, 1, 2, 3, and 4.
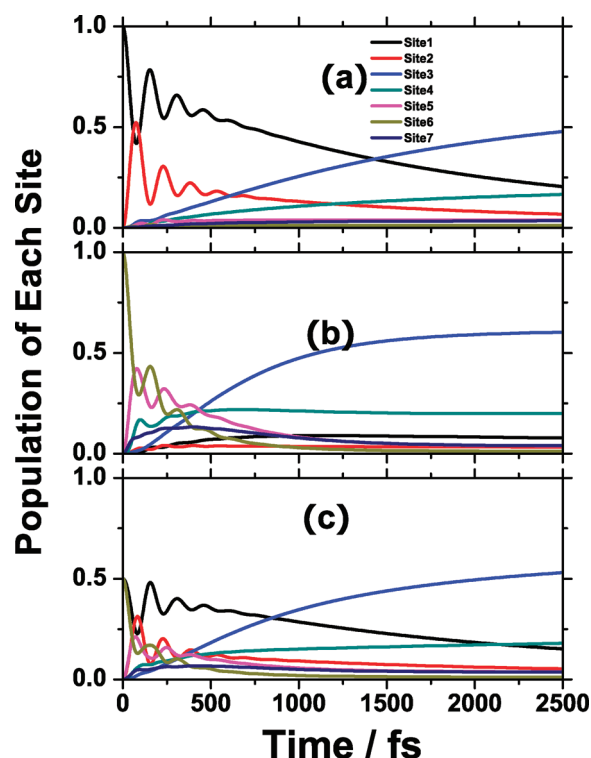

Figure 5. Long time dynamics of the population at each site for T = 77 K, where parts a, b, and c correspond to different initial conditions as noted before. All other parameters are the same as those in Figure 3.

smaller γ is, the longer the population beating can last. When γ^{-1} = 166 fs, the population beating time can last almost 700 fs. The main pathways for all cases are the same as the pathways at low temperature. Furthermore, the time evolution of the population for each site also converges to thermal equilibrium. However, the entire system reaches thermal equilibrium considerably sooner at room temperature. For example, the system initialized at site 6 reaches equilibrium at 1.5 ps when T = 300 K, compared to 2 ps at 77 K.

Behavior of the Auxiliary Density Operators. In order to further investigate the effects of the ADOs and their role in the
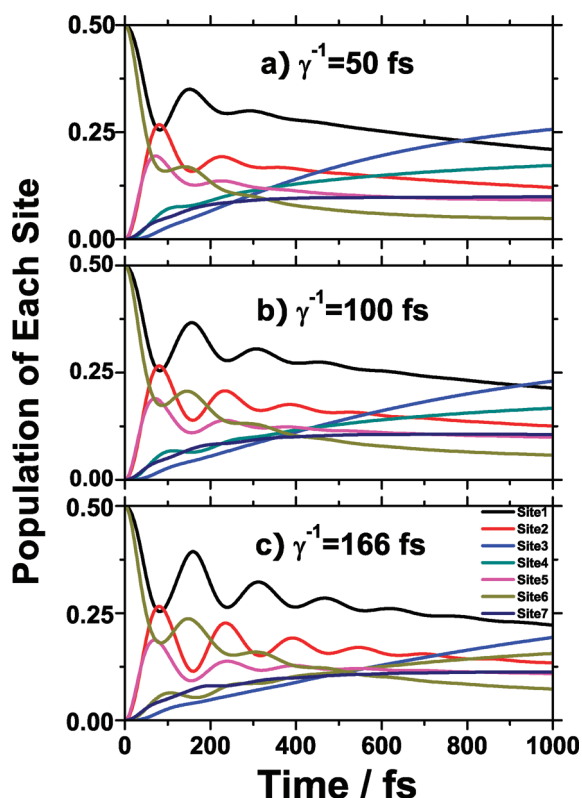
Figure 6. Population of all FMO sites at $T = 300$ K. The initial state is the superposition of sites 1 and 6. The reorganization energy remains 35 cm^{-1}. Three different values of phonon relaxation time are tested, which are $\gamma^{-1} = 50$ fs (a), $\gamma^{-1} = 100$ fs (b), and $\gamma^{-1} = 166$ fs (c).
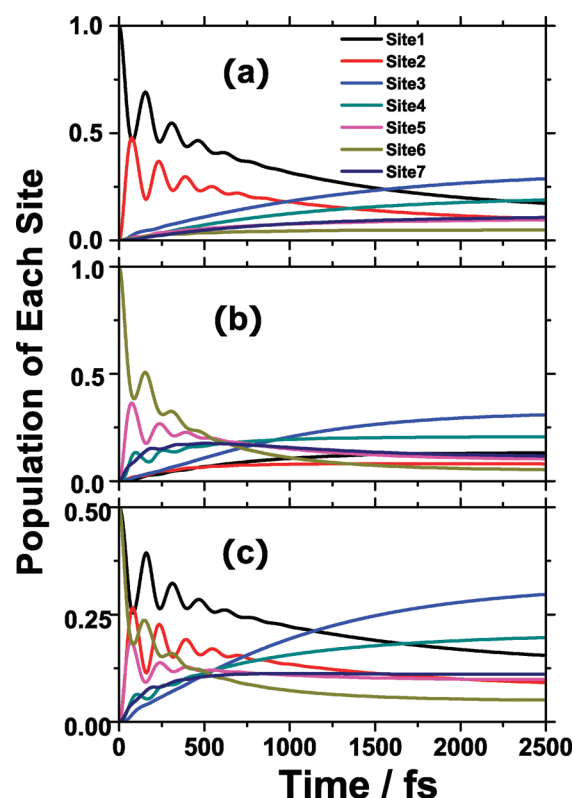

Figure 7. Long time evolution of the population of each site at $T = 300$ K, where parts a, b, and c correspond to site 1 initially excited, site 6 excited, and the superposition of sites 1 and 6. The reorganization energy is $\lambda_j = \lambda = 35$ cm^{-1}, and the Drude decay constant is $\gamma_j^{-1} = \gamma^{-1} = 166$ fs.

modified HEOM scheme, we examine the magnitude of their population elements and find that the majority of them are close to 0. However, there are some nonzero ADO elements during the time evolution. We plot their time dependence in Figure 4. For the case where site 1 is initially excited, the simulation shows that the most important ADO elements are $\langle 1|\rho_{n000000}|1\rangle$, with $n = 1$, 2, 3, and 4. For the site 6 initially excited case, the important ADOs are $\langle 6|\rho_{00000m0}|6\rangle$, with $m = 1$, 2, 3, and 4. From the image (Figure 4), it can be found that the amplitude of the ADOs decays rather quickly as the level of truncation increases. Conversely, the ADO populations are related to the amplitude of the site population in the RDO. When the population goes up, the corresponding population in ADOs also increases. For odd truncation levels ($\rho_{1000000}$, $\rho_{3000000}$, $\rho_{0000010}$, and $\rho_{0000030}$), the ADOs yield negative population. The results are indicative of the fact that the scaled HEOM approach reduces the amplitude of ADOs as the truncation level increases. Interestingly, there are no negative population elements of the density matrix when the truncation level of the correlation function is $K = 0$ at cryogenic temperature. This is in contrast to the original hierarchical approach,[7] in which some populations become negative.

Energy Transfer Pathways. We briefly comment on the exciton transfer pathways. The pathways are determined by the system Hamiltonian rather than by the system−environment coupling or the environment.[7,28] From Figures 3, 5, 6, and 7, we find that the frequency of the site population oscillations is independent of the temperature and bath relaxation rate. For example, in the pathway site 1 $\rightleftharpoons$ 2 $\rightarrow$ 3 and 4, the main beatings between sites 1 and 2 are caused by several features. The energy

barrier between sites 1 and 2 ($\Delta\varepsilon_{12} = -120$ cm^{-1}) is smaller than that between sites 1 and 6 ($\Delta\varepsilon_{16} = -220$ cm^{-1}), and the coupling of sites 1 and 2 is stronger. The population oscillation between sites 3 and 4 is due to the similar site energies and the strong coupling between them. In the real biological system, the RC is close to sites 3 and 4. When the exciton transfers to these sites, it moves to the RC directly and cannot return to the system. Other pathways start from site 6, i.e., site 6 $\rightleftharpoons$ 7 $\rightarrow$ 3 and 4, site 6 $\rightleftharpoons$ 5 $\rightarrow$ 3 and 4, and site 6 $\rightarrow$ 3 and 4. Although the population distribution is the same for all pathways at long times, the excitation transfer time is shorter for an initial excitation at site 6.[28] For the pathway of site 1, the site energy of site 2 is bigger than that of site 1. It is hard for the excitation to move from site 1 to site 2, and that is why the wave-like evolution lasts for a longer time. However, in the population pathway that starts from site 6, the excitation flows from the higher- to lower-energy sites all the time. This reduces the transfer time, and the system reaches thermal equilibrium faster. Comparing the two different temperatures in terms of the excitation transfer pathways, we note that the influence of the thermal bath is much stronger at room temperature than at low temperature. The bath at 300 K helps the system transfer the excitation more efficiently by reducing the quantum beating, thus speeding up the overall transfer times to the reaction center.

IV. CONCLUSION

In summary, we have examined the full dynamics of the transfer of excitation energy toward the reaction center through

the Fenna—Matthews—Olson (FMO) pigment—protein complex, employing the modified scaled hierarchical approach recently developed by Shi et al.[20] The scaled HEOM approach not only reduces the cutoff for the tier of auxiliary density operators but also decreases the truncation level of the correlation function, which makes it more efficient compared to the original HEOM approach. We have shown that a tier cutoff of $N_c = 4$ and a correlation function cutoff of $K = 0$ optimizes the simulation efficiency and accuracy for the parameter regime of the FMO complex. Furthermore, our theoretical results show that the population beating can last as long as 650 fs under cryogenic temperature (77 K). When the temperature is 300 K, the beating time can vary from 400 to 700 fs, depending on the environment parameters. Our simulation result is in accord with the conclusion of Ishizaki et al.[7] The improved computational performance of our scaled HEOM approach will be especially useful in theoretical studies of transport measures, such as efficiency, transfer time, and other properties, like entanglement. Moreover, this efficient approach also provides us with the potential to couple other effects into our current system. Under the current model, only the thermal effect is fully considered; however, many other effects exist in the real biological system, such as dipole—dipole interaction, the different phonon environment for each site, and slow structure changes of the FMO complex. It will be our future task to build a model with these features and examine the time evolution of entanglement and related quantum information measures.[35—39]

■ AUTHOR INFORMATION

Corresponding Author
*E-mail: kais@purdue.edu.

■ ACKNOWLEDGMENT

■ REFERENCES

(1) Andrews, D. L.; Demidov, A. A. *Resonance Energy Transfer*; Wiley: England,1999.

(2) Savikhin, S.; Buck, D. R.; Struve, W. S. *Chem. Phys.* **1997**, *223*, 303–312.

(3) Engel, G. S.; Calhoun, T. R.; Read, E. L.; Ahn, T. K.; Mancal, T.; Cheng, Y. C; Blanken-ship, R. E.; Fleming, G. R. *Nature* **2007**, *446*, 782–786.

(4) Mohseni, M.; Rebentrost, P.; Lloyd, S.; Aspuru-Guzik, A. *J. Chem. Phys.* **2008**, *129*, 174106.

(5) Rebentrost, P.; Mohseni, M.; Kassal, I.; Lloyd, S.; Aspuru-Guzik, A. *New J. Phys.* **2009**, *11*, 033003.

(6) Rebentrost, P.; Mohseni, M.; Aspuru-Guzik, A. *J. Phys. Chem. B* **2009**, *113*, 9942–9947.

(7) Ishizaki, A.; Fleming, G. R. *Proc. Natl. Acad. Sci. U.S.A.* **2009**, *106*, 17255–17260.

(8) Ishizaki, A.; Fleming, G. R. *J. Chem. Phys.* **2009**, *130*, 234111.

(9) Cho, M. H.; Vaswani, H. M.; Brixner, T.; Stenger, J.; Fleming, G. R. *J. Phys. Chem. B* **2005**, *109*, 10542–10556.

(10) Strumpfer, J.; Schulten, K. *J. Chem. Phys.* **2009**, *131*, 225101.

(11) Sarovar, M.; Ishizaki, A.; Fleming, G. R.; Whaley, K. B. *Nat. Phys.* **2010**, *6*, 462–467.

(12) Caruso, F.; Chin, A.; Datta, A.; Huelga, S.; Plenio, M. *Phys. Rev. A* **2010**, *81*, 062346.

(13) Lee, H.; Cheng, Y. C; Fleming, G. R. *Science* **2007**, *316*, 1462–1465.

(14) Sension, R. J. *Nature* **2007**, *446*, 740–741.

(15) Volkovich, R.; Toroker, M. C; Peskin, U. *J. Chem. Phys.* **2008**, *129*, 034501.

(16) Cheng, Y. C; Fleming, G. R. *Annu. Rev. Phys. Chem.* **2009**, *60*, 241–262.

(17) Collini, E.; Wong, C. Y.; Wilk, K. E.; Curmi, P. M. G.; Brumer, P.; Scholes, G. D. *Nature* **2010**, *463*, 644–U69.

(18) Scholes, G. D. *J. Phys. Chem. Lett.* **2010**, *1*, 2–8.

(19) Hoyer, S.; Sarovar, M.; Whaley, K. B. *New J. Phys.* **2010**, *12*, 065041.

(20) Shi, Q.; Chen, L. P.; Nan, G. J.; Xu, R. X.; Yan, Y. J. *J. Chem. Phys.* **2009**, *130*, 084105.

(21) Tanimura, Y.; Kubo, R. *J. Phys. Soc. Jpn.* **1989**, *58*, 101–114.

(22) Tanimura, Y.; Wolynes, P. G. *Phys. Rev. A* **1991**, *43*, 4131–4142.

(23) Fenna, R. E.; Matthews, B. W. *Nature* **1975**, *258*, 573–577.

(24) Li, Y. F.; Zhou, W. L.; Blankenship, R. E.; Allen, J. P. *J. Mol. Biol.* **1997**, *271*, 456–471.

(25) Camara-Artigas, A.; Blankenship, R. E.; Allen, J. P. *Photosynth. Res.* **2003**, *75*, 49–55.

(26) Ben-Shem, A.; Prolow, F.; Nelson, N. *FEBS Lett.* **2004**, *564*, 274–280.

(27) Tronrud, D. E.; Wen, J. Z.; Gay, L.; Blankenship, R. E. *Photosynth. Res.* **2009**, *100*, 79–87.

(28) Adolphs, J.; Renger, T. *Biophys. J.* **2006**, *91*, 2778–2797.

(29) Ishizaki, A.; Tanimura, Y. *J. Phys. Soc. Jpn.* **2005**, *74*, 3131–3134.

(30) Xu, R. X.; Cui, P.; Li, X. Q.; Mo, Y.; Yan, Y. J. *J. Phys. Chem.* **2005**, *122*, 041103.

(31) Tanimura, Y. *J. Phys. Soc. Jpn.* **2006**, *75*, 082001.

(32) Ishizaki, A.; Tanimura, Y. *J. Phys. Soc. Jpn.* **2005**, *74*, 3131–3134.

(33) Read, E. L.; Schlau-Cohen, G. S.; Engel, G. S.; Wen, J. Z.; Blankenship, R. E.; Fleming, G. R. *Biophys. J.* **2008**, *95*, 847–856.

(34) Panitchayangkoon, G.; Hayes, D.; Fransted, K. A.; Caram, J. R.; Harel, E.; Wen, J.; Blankenship, R. E.; Engel, G. S. *Proc. Natl. Acad. Sci. U.S.A.* **2010**, *107*, 12766–12770.

(35) Kais, S. *Reduced-density-matrix Mechanics - With Application To Many-electron Atoms and Molecules*; Wiley: Canada, 2007; Vol. 134, pp 493–535.

(36) Wei, Q.; Kais, S.; Chen, Y. P. *J. Chem. Phys.* **2010**, *132*, 121104.

(37) Xu, Q.; Kais, S.; Naumov, M.; Sameh, A. *Phys. Rev. A* **2010**, *81*, 022324.

(38) Plenio, M. B.; Huelga, S. F. *New J. Phys.* **2008**, *10*, 113019.

(39) Caruso, F.; Chin, A. W.; Datta, A.; Huelga, S. F.; Plenio, M. B. *J. Chem. Phys.* **2009**, *131*, 105106.

1537

dx.doi.org/10.1021/jp109559p |*J. Phys. Chem. B* 2011, 115, 1531–1537